1 # Electronic Supporting Information (ESI)

2

3 **Influence of catalyst zeta potential on the activation of persulfate**

4

5 Daniele Silvestri, [a] Kamil Krawczyk, [a] Mirosława Pawlyta, [b] Maciej Krzywiecki, [c] Vinod V.T. Padil, [a] Rafael Torres-

6 Mendieta, [a] Farshid Ghanbari, [d] Ozge Dinc, [e] Miroslav Černík, [a] Dionysios D. Dionysiou [f] and Stanisław Wacławek *[a]

7 [a] *Institute for Nanomaterials, Advanced Technologies and Innovation, Technical University of Liberec, Studentská 1402/2, 461 17 Liberec, Czech Republic;*

8 [b] *Materials Research Laboratory, Faculty of Mechanical Engineering, Silesian University of Technology, Konarskiego 18a St., 44–100 Gliwice, Poland;*

9 [c] *Institute of Physics – CSE, Silesian University of Technology, Konarskiego 22B, 44-100 Gliwice, Poland;*

10 [d] *Department of Environmental Health Engineering, Abadan Faculty of Medical Sciences, Abadan, Iran;*
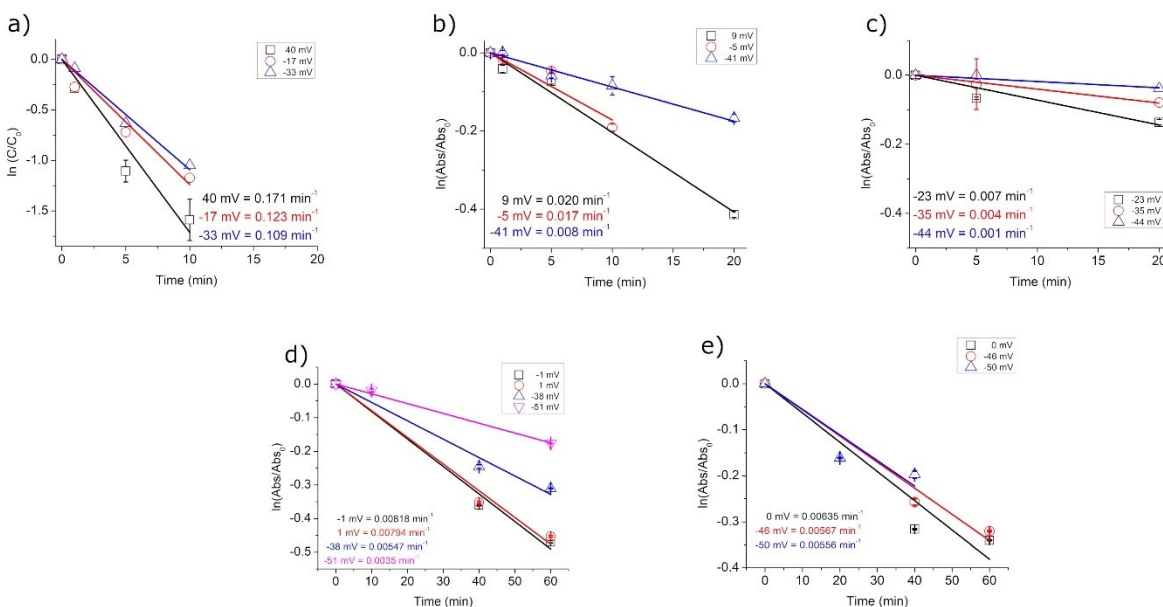
11 [e] *Department of Biotechnology, Hamidiye Health Science Institute, University of Health Sciences-Turkey, 34668, Uskudar, Istanbul, Turkey;*

12
13 [f] *Environmental Engineering and Science Program, Department of Chemical and Environmental Engineering (ChEE), University of Cincinnati, Cincinnati, OH 45221-0012, USA;*

14 *Corresponding author: stanislaw.waclawek@tul.cz*

15

16

17

18

19

20

21

22

23

24

25

26

27

28

29

# Contents

48

**Fig. S1** Time-dependent change of the natural logarithm of the normalized concentration of a) SMX (pH 3.0-5.0) or normalized absorbance b) MO (pH 7.0), and c) 4-NP (pH 11.0) due to oxidation by activated PDS by nZVI (along with various zeta potential values); time-dependent change of the natural logarithm of the normalized absorbance of MO (pH 3.0, 5.0 and 7.0) due to oxidation by activated PDS by d) GO and rGO and oxidation by PDS activated with e) FW 200 MO (pH 3.0, 5.0 and 7.0).

49

# Materials and methods

## Reagents and solutions

Chitosan (CS, 75-85% deacetylated, low molecular weight 50,000-190,000 Da), Poly(acrylic acid) (PAA, molecular weight 450,000 Da), 4-nitrophenol (≥99%), sodium hydroxide (≥97%), hydrochloric acid (37%), Methyl Orange (85% dye content), sulfamethoxazole and graphene oxide (GO; 2 mg/mL dispersion in $H_2O$) were purchased from Sigma-Aldrich (Czech Republic). Nitric acid (65%) and sodium peroxydisulfate (PDS, persulfate, 99%) were purchased from Lach-Ner (Czech Republic). Colour Black (FW 200) was manufactured by Degussa Corporation. Deionized water (18.2 MΩ·cm, ELGA, Veolia Water, Marlow, UK) was used in all experiments.

## Nanoparticles and reagent preparation

As a nZVI source, a commercial nanoscale zero-valent iron (Nanofer, Czech Republic) was used and modified by two different polymers, chitosan (CS) and polyacrylic acid (PAA). The pristine nZVI stock solution (20 %wt.) was prepared by dispersion of nZVI powder in DI water under a nitrogen atmosphere in a DL 05 Laboratory Dispersion Unit (NANOIRON, CZ). Then, the nanoparticles were washed three times by DI water. The nZVI concentration in the stock solution was determined by an nZVI tester (NANOIRON, CZ; ZVI determination section in the supplementary information).[1]

Chitosan solution was prepared by mixing in acidified (nitric acid) DI water for 30 min until a clear mixture was obtained. The CS solution (2%) and nZVI (20%) were stirred in the nitrogen atmosphere of the DL 05, then washed three times in DI water. A similar

66    procedure was followed to prepare the PAA-nZVI samples (without acidification). All samples were freeze-dried and stored in a

67    desiccator, unless stated otherwise. Detailed characterization of the various nZVI samples is provided below, i.e., scanning

68    electron microscopy (SEM), transmission electron microscopy (TEM) (Fig. S2), energy-dispersive X-ray spectroscopy (EDX) (Fig.

69    S3), thermo-gravimetric analysis (TGA) (Fig. S4), X-ray photoelectron spectroscopy (XPS) (Figs. S5 and S6), ZVI content (Fig. S7)

70    and estimation of the specific surface area by differential centrifugal sedimentation (DCS) (Table S1).

71    A commercial GO solution (2 mg/mL) was used by simple dilution to obtain the desired concentrations. Material characterization

72    can be found on the Sigma Aldrich supplier website.

73    Reduced graphene oxide (rGO) was created by following the procedure reported previously by Sieradzka et al.[2] Briefly, 4 g of GO

74    were placed in a thermal reduction chamber filled with nitrogen. Then, the chamber was heated (30 °C/min) until micro-explosion

75    occurred. A detailed synthesis procedure and characterization of rGO is provided by Sieradzka et al.[2]

76    A commercial carbon FW 200 was used as another carbonaceous material. Detailed characterization was provided in the article

77    of Pawlyta et al.[3]

## Activation of persulfate

79    The activation of PDS was performed with three different surface-modified nZVI and three different carbonaceous materials.

80    Three different pollutants were tested to understand the correlation between the catalyst zeta potential and the radical

81    production rate from PDS. While the SMX oxidation test was performed at pH 3.0 and 5.0, the MO oxidation experiment (for

82    nZVI) was performed in a near-neutral pH (and in various pH values for the carbonaceous materials), and 4-nitrophenolate at pH

83    11.0. During the reaction at high pH, the pH gradually turned more acidic, which is typical behavior of PDS systems.[4] This

84    methodology for testing the influence of the zeta potential of catalysts on the reactivity of the system has also been described

85    elsewhere.[5] The reaction kinetics were fitted using the pseudo-first-order kinetic model.[6] All the surface-modified nZVI were

86    created in such way that the variances in size, morphology and ZVI content would be minimal. Therefore, the differences in rate

87    constants could practically be assigned solely to the different surface properties of the nZVI.

88    The tests were conducted in triplicate, and the error bars represent the standard deviation of such data set.

## Sulfamethoxazole oxidation

90    The sulfamethoxazole (SMX) stock solution was prepared by dissolving 20 mg of SMX in 1 L of DI water and stirring for 40 min in

91    a volumetric flask. For the catalytic test, SMX, PDS, and nZVI were added to the reaction mixture (volume of 20 mL) to reach the

92    concentrations of 10 mg/L, 2 mM, and 0.3 g/L, respectively. The reaction mixture was stirred for the duration of the test. For the

93    sampling, 1 mL of the solution was taken and filtered using a syringe filter (PTFE, 0.22 μm), then the samples were analyzed by

94    high-performance liquid chromatography (HPLC; UltiMate 3000, Thermo Fisher Scientific, Czech Republic), composed of an

95    isocratic pump, degasser, autosampler, column oven, and UV-Vis (VWD-3100) as a detector. SMX was separated by a Reprospher

96    C18 column (150 × 4.6 mm, 3 μm) heated to 40 °C, and a filtered mobile phase consisting of methanol and DI water at a ratio of

97    1:1 (v/v) with a flowrate of 1 mL/min and pH adjusted to 3.0 by $H_3PO_4$. The tests were conducted at a pH of 3.0 and 5.0 without

98    a buffer (addition of sulfuric acid). The synthesized nZVI used for this test was CS-nZVI (pH 5.0) and PAA-nZVI (pH 3.0 and 5.0).

## Methyl Orange oxidation

The Methyl Orange (MO) stock solution was prepared by dissolving 10 mg of MO in 100 mL of DI water in a volumetric flask and stirring for 5 min. For the catalytic test, MO, PDS and nZVI/GO/rGO/FW 200 were added to the reaction mixture to reach the final concentrations of 50 mg/L, 1 mM, and 0.2/0.05/0.05/0.05 g/L, respectively. The reaction mixture was stirred for the duration of the test (10 min for nZVI and 60 min for carbonaceous materials). In order to analyze the samples, 1 mL of solution was taken and filtered by a syringe filter (PTFE, 0.22 μm), then the samples were analyzed by a Vis spectrophotometer (DR 3900, HACH LANGE s.r.o., Czech Republic) at a wavelength of 464 nm in a 1 cm cuvette. The general procedure and wavelength used for this test are based on the literature.[7] All tests were conducted at an initial pH of 7.0 and without a buffer. In contrast, carbonaceous materials were tested at pH of 3.0, 5.0 and 7.0. pH was adjusted by adding HCl (1 M).

## 4-nitrophenolate oxidation

A 4-nitrophenolate (4-NP) stock solution (5 mM of 4-nitrophenol in 10 mL of DI water) was prepared by adding 0.1 mL of NaOH (1 M) to adjust the pH to 11.0. For the catalytic test, 4-NP, PDS and nZVI were added to the reaction mixture to reach the final concentrations of 0.12 mM, 1 mM, and 0.2 g/L, respectively. The reaction mixture was stirred for the duration of the test. The samples were taken into 1 cm quartz cuvettes, filtered using syringe filters (PTFE, 0.22 μm), and detected by the Vis spectrophotometer (DR 3900, HACH LANGE s.r.o., Czech Republic) at a wavelength of 401 nm. It should be noted that by alkalizing the 4-nitrophenol stock solution, the highest absorbance peak shifts from 317 nm to 401 nm due to the formation of 4-nitrophenolate. The modified procedure was based on the literature.[8]

# Analytical and characterization methodology

The morphology and composition of the nanoparticles were studied using a scanning electron microscope (SEM, Everhardt-Thornley, ZEISS, Ultra/Plus, Germany) with an acceleration voltage of 0.02 - 30 kV coupled with energy-dispersive X-ray spectroscopy (EDX, OXFORD, UK) for determination of the various elements in the synthesized nanoparticles.

Further characterization was performed on an aberration-corrected field-emission transmission electron microscope (TEM, FEI Titan 80–300 TEM/STEM, FEI, USA) operated at 300 kV and equipped EDS spectrometer.

Thermal stability (TGA) and composition were determined by a Q500 instrument (TA Instruments, USA). The analysis was performed in a nitrogen atmosphere at a flow rate of 60 mL/min. The sample was heated from 30 to 500 °C.

X-ray photoelectron spectroscopy analysis (XPS) was performed using a multi-chamber ultra-high vacuum experimental setup (base pressure $8 \cdot 10^{-8}$ Pa) equipped with a hemispherical electron energy analyzer (PREVAC EA15, PREVAC sp. z o.o., Poland) fitted with a 2D-MCP detector. Samples for analysis were irritated with the energy of 1486.6 eV provided by an Al Kα X-ray source PREVAC dual anode XR-40B. The binding energy scale of the analyzer was calibrated to Ag $3d_{5/2}$ (368.2 eV).[9] For survey spectra the pass energy (PE) was set to 200 eV, while for particular energy regions PE 100 eV was used. Data were fitted with the use of CASA XPS® embedded algorithms. The particular energy regions were fitted with components represented as a product of Gaussian (70%) and Lorentzian (30%) lines except for Iron $Fe^0$ where Gaussian and Lorentzian product was supplemented with asymptotic blend representing the metallic nature of the component. Shirley function was utilized for the background subtraction.

133  A commercial kit was used to determine the $Fe^{2+}$ concentration (Lange LCK 320). Briefly, the samples were first filtered by a
134  syringe filter (0.22 μm), then 2 mL of the filtered solution were added to the reaction tube and mixed for 5 minutes (a dilution
135  was applied if necessary). The concentration was determined by a Vis spectrophotometer (DR 3900, HACH LANGE s.r.o., Czech
136  Republic).

137  A Vis spectrophotometer (DR 3900, HACH LANGE s.r.o., Czech Republic) was used for the sample absorbance measurements. The
138  zeta potential of dispersed particles was analyzed by a Zetasizer Nano ZS (Malvern PANalytical Ltd, United Kingdom) with an
139  autocorrelation function of 10 seconds. Samples for analysis were prepared in a DI water suspension and in triplicate. The pH
140  levels were adjusted either by NaOH or HCl.

141  A differential centrifugal sedimentation (DCS) instrument (DC24000UHR, CPS Instruments Inc., USA) was used to analyze particle
142  size distribution. The instrument operated at the disc rotation speed of ~5000 rpm and in 8–24% (w/w) sucrose density gradient.
143  The instrument was calibrated using the PVC nanosphere standard (1.4 μm) before the beginning of each measurement.

# Characterization of nZVIs

## SEM, TEM and EDX

146  The nanoparticles with and without polymers were analyzed by scanning electron microscope (SEM) and transmission electron
147  microscope (TEM) to get information about the morphology and particle size. All samples showed chain-like structures (Fig. S2).
148  This structure could be due to the physical attraction of these nanoparticles, which is typical for nano zero-valent iron (nZVI).
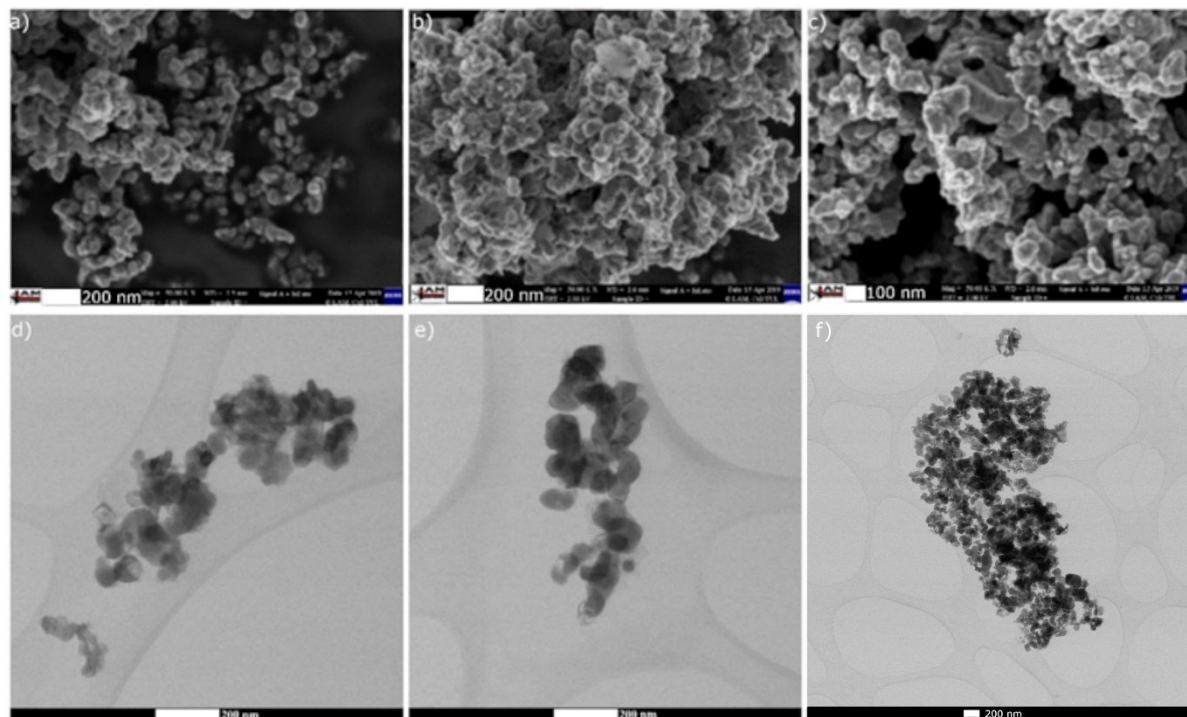


**Fig. S2** SEM images of a) nZVI, b) CS-nZVI and c) PAA-nZVI, TEM images of d) nZVI, e) CS-nZVI and f) PAA-nZVI.

149  Based on SEM and TEM analysis, there were not found substantial differences between these nanoparticles.

150   The presence of both oxygen and iron on the surface of the pristine nZVI was detected using EDX analysis (Fig. S3a), indicating a
151   core-shell structure consisting of a thin layer of oxidized iron at the surface and zero-valent iron in the core.[10] EDX of CS-nZVI and
152   PAA-nZVI (Fig. S3b,c) showed an additional peak ascribed to carbon, and the presence of carbon on the surface of these
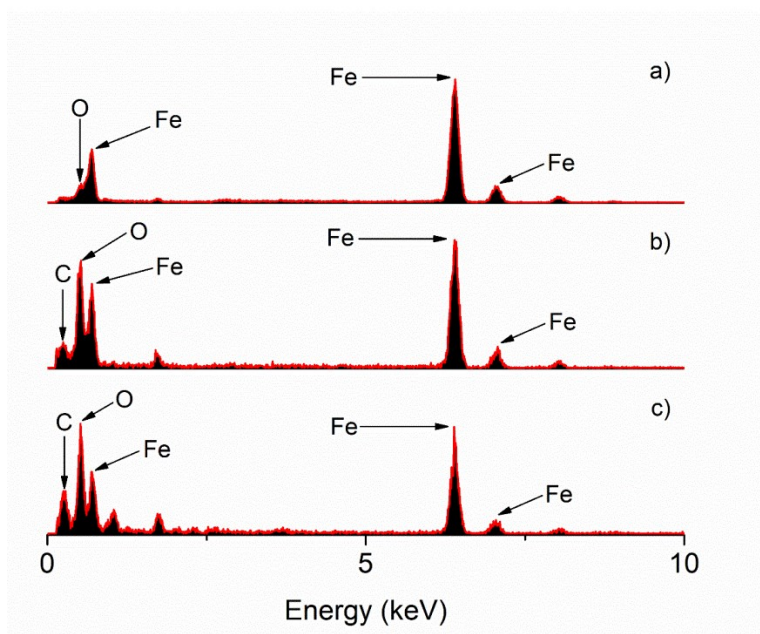153   nanoparticles might be attributed to the polymers.



**Fig. S3** *EDX analysis of a) nZVI b) CS-nZVI and c) PAA-nZVI.*

154

## TGA

156   Thermogravimetric analysis (TGA) was performed to study the mass changes of the samples with increasing temperature from
157   30 to 500 °C (Fig. S4). The TGA curve of pristine nZVI had no weight loss (30-500 °C) due to the absence of organic compounds on
158   the sample. While both samples CS-nZVI and PAA-nZVI showed a reduction in weight by 3.6 and 3.2%, respectively. In the TGA
159   curve of CS-nZVI, the initial weight loss recorded from ~30 to ~100 °C may be attributed to the loss of moisture since the sample
160   did not show an additional weight loss until ~250 °C. A dramatic weight loss recorded between ~250 °C and ~430 °C may be due
161   to further dehydration of the sample and deacetylation and depolymerization of polymers as reported previously by de Britto,
162   and Campana-Filho.[11] In the case of PAA-nZVI, the first stage of weight loss (from ~40 to ~180 °C) may be due to the loss of
163   moisture, while the second weight loss that occurred between ~300 and ~450 °C is in accordance with polymer
164   dehydration/decarboxylation previously reported by Datsyuk et al.[12] By comparing the TGA of pristine nZVI and nZVI coated by
165   polymers, it may be assumed that both polymers are present as a coating of the nanoparticles. This analysis is in agreement with
166   the EDX analysis reported in this work. It should be noted that the weight loss observed by the TGA analysis was similar for both
167   samples, indicating that the nanoparticles were coated with a similar amount of polymer.
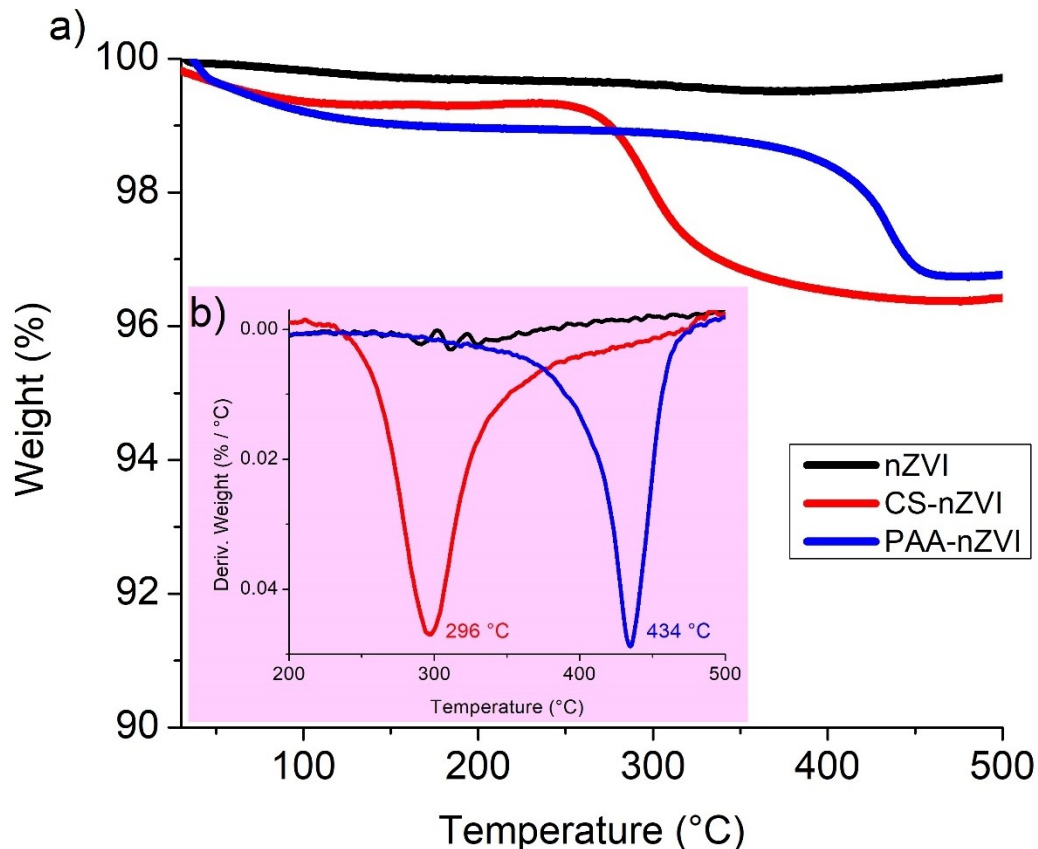
**Fig. S4** *a) TGA curve of pristine nZVI, CS-nZVI and PAA-nZVI and b) derivative thermogravimetric (DTG) curves of the respective samples.*

168

## XPS

The XPS analyses of both CS-nZVI and PAA-nZVI are shown in Figure S5. For a better understanding of the structure of the nZVI, a wide survey and high-resolution scan of Fe 2p (Fig. S5) and C1s (Fig. S6) were performed. The wide scan analysis for both samples (Fig. S5a) showed major peaks (Fe 2p, O1s and C1s) ascribed to Fe, O and C.

The presence of both carbon and oxygen could be due to the polymer layer on the iron surface. These two peaks were definitive confirmation of EDX analysis and the presence of polymer on synthesized nanoparticles. In the CS-nZVI high-resolution spectrum of Fe 2p (Fig. S5b I) four peaks ascribed to the oxidation state of iron[13,14] could be observed, while at ~706 eV associated satellite peak could be attributed to $Fe^0$ according to the literature.[13,15] The small peak of $Fe^0$ could be due to the core shell structure of these nanoparticles. XPS analysis showed only the surface characteristic of the sample due to limited photoelectron information depth (the majority signal for Fe 2p is originating from ~5 nm).

179    Therefore, the presence of an iron oxide layer showed more intensity compared to the $Fe^0$ peak. The oxide-related components
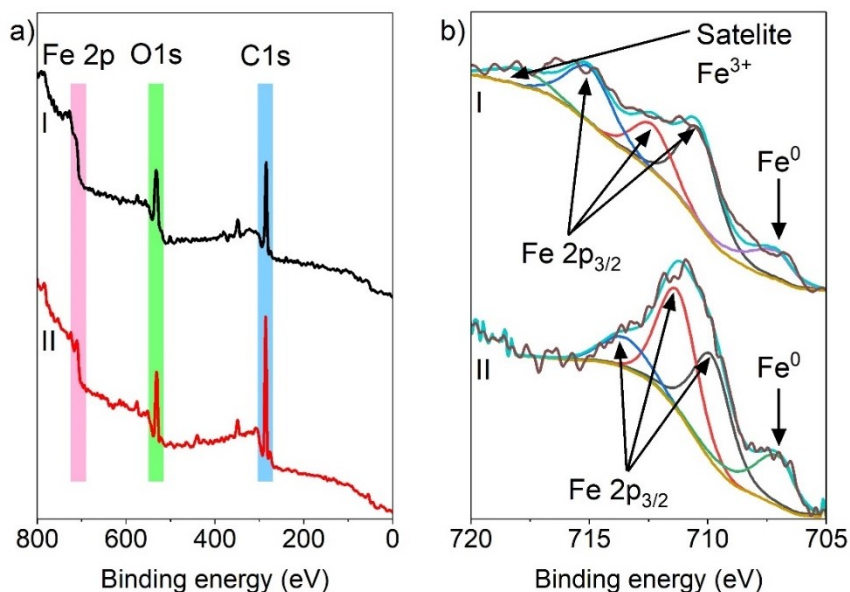
180    are representing both, $Fe^{2+}$ and $Fe^{3+}$ states together with the satellite features at the higher binding energy side.

181

182    In PAA-nZVI Figure S5b II), similar results could be observed as for the CS-nZVI. Most of the peaks can be attributed to the iron

183    oxidation states i.e., $Fe^{2+}$ and $Fe^{3+}$, while the peak at ~706 eV represents $Fe^0$. Also, in this case, the XPS implied a core shell

184    structure of these nanoparticles with an oxide layer on the surface and $Fe^0$ as the core. Crucial results can be deduced from the

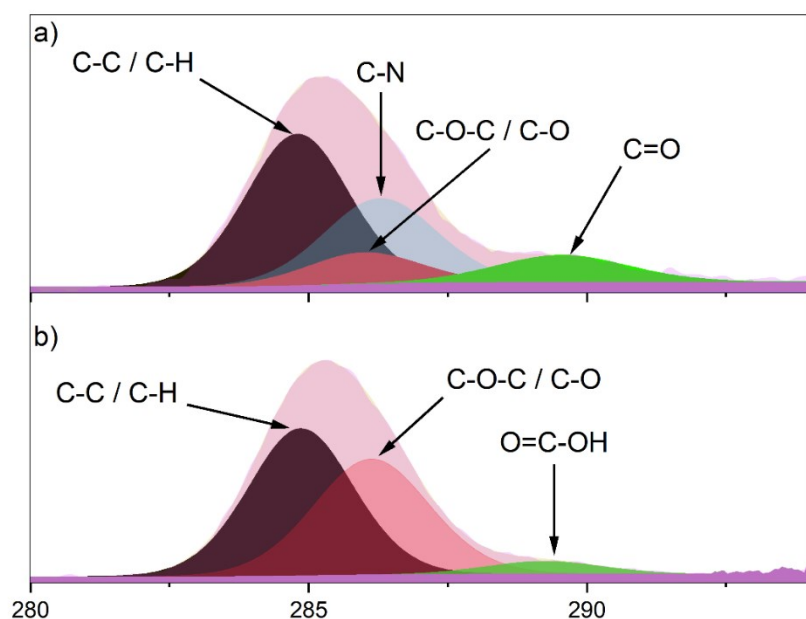185    C1s high resolution spectra of both nanoparticles (Fig. S6a,b).

**Fig. S6** *C1s high resolution XPS spectra of a) CS-nZVI and b) PAA-nZVI*

186

187   In CS-nZVI (Fig. S6a) the peak at ~285 eV could be ascribed to C-C / C-H , which confirms the presence of aliphatic compound as

188   reported previously by Li and co-workers[16], while the peaks at ~286 eV could be assigned to C-N and C-O-C / C-O groups. At ~289

189   eV, the last peak shown could be assigned to the C=O and residue signal of group. Figure S6b) shows the C1s high-resolution

190   spectra of PAA-nZVI. The peak at ~285 eV could be assigned to C-C configuration and to the hydrocarbon backbone of the

191   polymer.[17,18] While, the peak at ~286 eV could be ascribed to C-O-C / C-O group,[19] and the peak at ~289 eV represented the

192   carboxylic groups on PAA.[17]

## ZVI determination

194   The ZVI content (Fig. S7) was measured by a nZVI tester (NANO IRON, Czech Republic). ZVI was determined based on the chemical

195   reaction between $Fe^0$ and $K_2SO_4$, from which hydrogen is produced (Eq. S1):[1]

196   $2KHSO_4 + Fe^0 \rightarrow FeSO_4 + K_2SO_4 + H_2$ (g)                                            (S1)

197　Based on this analysis, it is possible to state that the synthesized irons did not differ significantly in their ZVI content.

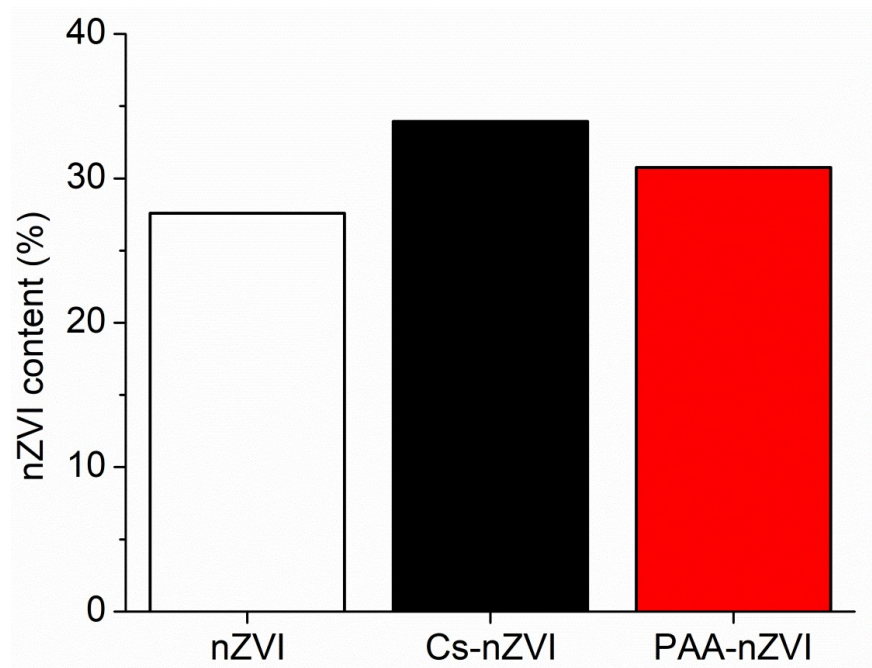198　Nonetheless, for the degradation experiments, the samples were appropriately diluted.



**Fig. S7** *ZVI content in the nZVI, CS-nZVI and PAA-nZVI samples*

## nZVIs specific surface area

199

200　In order to test any changes in the nature of the catalysts after use, a size distribution analysis was performed (DSC) before and
201　after the reaction. Relying on the fact that the density of the particles is the same as that of the bulk material,[20] the specific
202　surface area (SSA) of particles was estimated [basing on the equation: SSA = $6000/d \cdot \rho$; Where d is the diameter (nm) and $\rho$ is the
203　density of particles (g/cm$^3$)],[6,20] and presented in table S1.

204　From this analysis, it is evident that the SSA does not change significantly after the catalytic reaction as well as during the testing
205　of the same particles at various solution pH values.

206　Table S1. Estimation of the specific surface area (SSA) of nZVI particles before and after the reaction in various environments.

|  | SSA (m$^2$/g) | |
| --- | --- | --- |
| **pH 3** | **Before** | **After** |
| CS-nZVI | 1.09 | 1.14 |
| PAA-nZVI | 1.21 | 1.23 |
| **pH 7** | **Before** | **After** |
| nZVI | 1.10 | 0.94 |
| CS-nZVI | 0.93 | 1.03 |
| PAA-nZVI | 1.34 | 1.17 |

| pH 11 | Before | After |
|---|---|---|
| nZVI | 1.34 | 0.94 |
| CS-nZVI | 0.93 | 0.98 |
| PAA-nZVI | 1.15 | 1.34 |

207

# Estimation of the number of superficial atoms in the samples

The number of superficial atoms that may be involved in the persulfate activation was estimated by comparing the number of atoms on the surface of the ZVI nanoparticles with the number of stabilizing compounds used. In the estimation, two essential conditions were considered: (i) a stabilizing compound would bind exclusively with one atom, and (ii) the number of atoms that are not contemplated for the binding are understood as the superficial atoms available for the persulfate activation.

Both values (Tables S1-3) were calculated based on the following assumptions: (i) the entire 3.6% of CS (mol. weight 50000 Da) and 3.2% of PAA (mol. weight 450000 Da) were attached to the CS-nZVI and PAA-nZVI, respectively, (ii) the shape of the nanoparticles was spherical, (iii) the surface of the nanoparticles was entirely composed of $Fe^0$, where the density was 7870 $kg/m^3$, and the atomic radii were 0.126 nm.

Using these calculations, it was possible to determine that the percentage of superficial atoms available for the persulfate activation was almost the same in all cases. After comparing with the non-equal oxidation rate constants in Fig. 2, it was deduced that the number of the available superficial atoms in the nanoparticles does not play a major role in the persulfate activation that leads to the oxidation of the pollutants, but the type of stabilization agent does.

Table S2. Data used to estimate chemically active sites for the oxidation of SMX through the catalytic activation of persulfate. The reaction volume was 20 mL, the nanoparticle concentration was 0.3 g/L, and the nanoparticle diameters were 84 nm for nZVI, 97 nm for CS-nZVI, and 115 nm for PAA-nZVI.

| Sample | No. of nanoparticles in reaction volume | Total surface of nanoparticles ($m^2$) | No. of atoms on the entire surface | No. of compounds attached to the surface of the nanoparticles | % of chemically active sites |
|---|---|---|---|---|---|
| nZVI | - | - | - | - | - |
| CS-nZVI | $1.53 \cdot 10^{12}$ | $4.54 \cdot 10^{-2}$ | $2.27 \cdot 10^{17}$ | $2.60 \cdot 10^{15}$ | 98.85 |
| PAA-nZVI | $9.27 \cdot 10^{11}$ | $3.85 \cdot 10^{-2}$ | $1.93 \cdot 10^{17}$ | $2.56 \cdot 10^{14}$ | 99.86 |

Table S3. Data used to estimate chemically active sites for the oxidation of MO through the catalytic activation of persulfate. The reaction volume was 20 mL, the nanoparticle concentration was 0.2 g/L, and the nanoparticle diameters were 84 nm for nZVI, 97 nm for CS-nZVI, and 115 nm for PAA-nZVI.

| Sample | No. of nanoparticles in reaction volume | Total surface of nanoparticles ($m^2$) | No. of atoms on the entire surface | No. of compounds attached to the surface of the nanoparticles | % of chemically active sites |
|---|---|---|---|---|---|
| nZVI | $1.64 \cdot 10^{12}$ | $3.63 \cdot 10^{-2}$ | $1.82 \cdot 10^{17}$ | - | 100 |

| | | | | | |
|---|---|---|---|---|---|
| CS-nZVI | $1.02 \cdot 10^{12}$ | $3.03 \cdot 10^{-2}$ | $1.52 \cdot 10^{17}$ | $1.73 \cdot 10^{15}$ | 98.85 |
| PAA-nZVI | $6.18 \cdot 10^{11}$ | $2.56 \cdot 10^{-2}$ | $1.29 \cdot 10^{17}$ | $1.66 \cdot 10^{14}$ | 99.87 |

228

Table S4. Data used to estimate chemically active sites for the oxidation of 4-NP through the catalytic activation of persulfate. The reaction volume was 10 mL, the nanoparticle concentration was 0.2 g/L, and the nanoparticle diameters were 84 nm for nZVI, 97 nm for CS-nZVI, and 115 nm for PAA-nZVI.

| Sample | No. of nanoparticles in reaction volume | Total surface of nanoparticles (m²) | No. of atoms on the entire surface | No. of compounds attached to the surface of the nanoparticles | % of chemically active sites |
|---|---|---|---|---|---|
| nZVI | $8.19 \cdot 10^{11}$ | $1.81 \cdot 10^{-2}$ | $9.10 \cdot 10^{16}$ | - | 100 |
| CS-nZVI | $5.13 \cdot 10^{11}$ | $1.28 \cdot 10^{-2}$ | $7.60 \cdot 10^{16}$ | $8.67 \cdot 10^{14}$ | 99.85 |
| PAA-nZVI | $3.09 \cdot 10^{11}$ | $1.51 \cdot 10^{-2}$ | $6.43 \cdot 10^{16}$ | $8.56 \cdot 10^{13}$ | 99.86 |

231

# References

233 1    J. Filip, J. Soukupova, J. Kaslfk, J. Slunsky and R. Zboril, in *Iron Nanomaterials for Water and Soil Treatment*, Jenny
234      Stanford Publishing, 2018, pp. 119–147.

235 2    M. Sieradzka, C. Ślusarczyk, R. Fryczkowski and J. Janicki, *J. Mater. Res. Technol.*, 2020, **9**, 7059–7067.

236 3    M. Pawlyta, J. N. Rouzaud and S. Duber, *Carbon*, 2015, **84**, 479–490.

237 4    H. Milh, B. Schoenaers, A. Stesmans, D. Cabooter and R. Dewil, *Chem. Eng. J.*, 2020, **379**, 122234.

238 5    S. Li, J. Tang, Q. Liu, X. Liu and B. Gao, *Environ. Int.*, 2020, **138**, 105639.

239 6    D. Silvestri, S. Wacławek, A. Venkateshaiah, K. Krawczyk, B. Sobel, V. V. T. Padil, M. Černík and R. S. Varma, *Carbohydr.*
240      *Polym.*, 2020, **232**, 115806.

241 7    S. Xie, P. Huang, J. J. Kruzic, X. Zeng and H. Qian, *Sci. Rep.*, 2016, **6**, 21947.

242 8    B. Baruah, G. J. Gabriel, M. J. Akbashev and M. E. Booher, *Langmuir*, 2013, **29**, 4225–4234.

243 9    NIST X-ray Photoelectron Spectroscopy (XPS) Database, Version 3.5 (https://srdata.nist.gov/xps/default.aspx)

244 10   J. Soukupova, R. Zboril, I. Medrik, J. Filip, K. Safarova, R. Ledl, M. Mashlan, J. Nosek and M. Cernik, *Chem. Eng. J.*, 2015,
245      **262**, 813–822.

246 11   D. de Britto and S. P. Campana-Filho, *Thermochim. Acta*, 2007, **465**, 73–82.

247 12   V. Datsyuk, L. Billon, C. Guerret-Piécourt, S. Dagréou, N. Passade-Boupatt, S. Bourrigaud, O. Guerret and L. Couvreur, *J.*
248      *Nanomater.*, 2007, 074769.

249 13   M. Fan, T. Li, J. Hu, R. Cao, Q. Wu, X. Wei, L. Li, X. Shi and W. Ruan, Materials, 2016, **9**, 687.

250 14   T. Yamashita and P. Hayes, *Appl. Surf. Sci.*, 2008, **254**, 2441–2449.

251 15   H. Xu, Y. Sun, J. Li, F. Li and X. Guan, *Environ. Sci. Technol.*, 2016, **50**, 8214–8222.

252 16   P. C. Li, G. M. Liao, S. R. Kumar, C. M. Shih, C. C. Yang, D. M. Wang and S. J. Lue, *Electrochim. Acta*, 2016, **187**, 616–628.

253 17   G. Speranza, L. Minati, S. Torrengo, B. Rossi, C. Migliaresi, D. Maniglio, and L. Dalbosco, *Adv. Sci. Technol.,* 2010, **76**,
254       165–70.

255 18   L. Li, Y. Da, S. Ying, W. Zheng, X. Zhang and X. Yu, *Polym. Bull.*, 2017, **74**, 505–516.

256 19   A. B. Ruiz-Muelle, R. Contreras-Cáceres, P. Oña-Burgos, A. Rodríguez-Dieguez, J. M. López-Romero and I. Fernández,
257       *Appl. Surf. Sci.*, 2018, **428**, 566–578.

258 20   C. Kästner and A. F. Thünemann, *Langmuir*, 2016, **32**, 7383–7391.

259